Measurements of the Electric Form Factor of the Neutron using the Reaction $^3\overrightarrow{\mathrm{He}}(\vec{\mathrm{e}},\mathrm{e'n})\mathrm{pp}$ up to $\mathrm{Q}^2 = 3.4$ GeV^2

S. Riordan,[1,2] S. Abrahamyan,[3] B. Craver,[1] A. Kelleher,[4] A. Kolarkar,[5] J. Miller,[6] G.D. Cates,[1] N. Liyanage,[1] B. Wojtsekhowski,[7,*] A. Acha,[8] K. Allada,[5] B. Anderson,[9] K. A. Aniol,[10] J.R.M. Annand,[11] J. Arrington,[12] T. Averett,[4] A. Beck,[13,7] M. Bellis,[2] W. Boeglin,[8] H. Breuer,[6] J.R. Calarco,[14] A. Camsonne,[7] J.P. Chen,[7] E. Chudakov,[7] L. Coman,[8] B. Crowe,[15] F. Cusanno,[16] D. Day,[1] P. Degtyarenko,[7] P.A.M. Dolph,[1] C. Dutta,[5] C. Ferdi,[17] C. Fernández-Ramírez,[18,19] R. Feuerbach,[7,4] L.M. Fraile,[19] G. Franklin,[2] S. Frullani,[16] S. Fuchs,[4] F. Garibaldi,[16] N. Gevorgyan,[3] R. Gilman,[20,7] A. Glamazdin,[21] J. Gomez,[7] K. Grimm,[4] J.-O. Hansen,[7] J.L. Herraiz,[19] D.W. Higinbotham,[7] R. Holmes,[22] T. Holmstrom,[4] D. Howell,[23] C.W. de Jager,[7] X. Jiang,[20] M.K. Jones,[7] J. Katich,[4] L.J. Kaufman,[24] M. Khandaker,[25] J.J. Kelly,[6,†] D. Kiselev,[26] W. Korsch,[5] J. LeRose,[7] R. Lindgren,[1] P. Markowitz,[8] D.J. Margaziotis,[10] S. May-Tal Beck,[13,7] S. Mayilyan,[3] K. McCormick,[27] Z.-E. Meziani,[28] R. Michaels,[7] B. Moffit,[4] S. Nanda,[7] V. Nelyubin,[1] T. Ngo,[10] D.M. Nikolenko,[29] B. Norum,[1] L. Pentchev,[4] C.F. Perdrisat,[4] E. Piasetzky,[30] R. Pomatsalyuk,[21] D. Protopopescu,[11] A.J.R. Puckett,[13] V.A. Punjabi,[25] X. Qian,[31] Y. Qiang,[13] B. Quinn,[2] I. Rachek,[29] R.D. Ransome,[20] P.E. Reimer,[12] B. Reitz,[7] J. Roche,[7] G. Ron,[30] O. Rondon,[1] G. Rosner,[11] A. Saha,[7] M. Sargsian,[8] B. Sawatzky,[28] J. Segal,[7] M. Shabestari,[1] A. Shahinyan,[3] Yu. Shestakov,[29] J. Singh,[1] S. Širca,[13] P. Souder,[22] S. Stepanyan,[32] V. Stibunov,[33] V. Sulkosky,[4] S. Tajima,[1] A.W. Tobias,[1] J.M. Udias,[19] G.M. Urciuoli,[16] B. Vlahovic,[15] H. Voskanyan,[3] K. Wang,[1] F.R. Wesselmann,[25] J. R. Vignote,[34] S.A. Wood,[7] J. Wright,[27] H. Yao,[31] and X. Zhu[13]

[1]University of Virginia, Charlottesville, VA 22903
[2]Carnegie Mellon University, Pittsburgh, PA 15213
[3]Yerevan Physics Institute, Yerevan 375036, Armenia
[4]College of William and Mary, Williamsburg, VA 23187
[5]University of Kentucky, Lexington, KY 40506
[6]University of Maryland, College Park, MD 20742
[7]Thomas Jefferson National Accelerator Facility, Newport News, VA 23606
[8]Florida International University, Miami, FL 33199
[9]Kent State University, Kent, OH 44242
[10]California State University Los Angeles, Los Angeles, CA 90032
[11]University of Glasgow, Glasgow G12 8QQ, Scotland, U.K.
[12]Physics Division, Argonne National Laboratory, Argonne, IL 60439
[13]Massachusetts Institute of Technology, Cambridge, MA 02139
[14]University of New Hampshire, Durham, NH 03824
[15]North Carolina Central University, Durham, NC 27707
[16]INFN gr. Sanità coll. Sezione di Roma and Istituto Superiore di Sanità, Rome, Italy
[17]Université Blaise Pascal/IN2P3, F-63177 Aubière, France
[18]European Centre for Theoretical Studies in Nuclear Physics and Related Areas (ECT), I-38050 Villazzano (TN), Italy*
[19]Universidad Complutense de Madrid, Madrid, Spain
[20]Rutgers, The State University of New Jersey, Piscataway, NJ 08854
[21]Kharkov Institute of Physics and Technology, Kharkov 61108, Ukraine
[22]Syracuse University, Syracuse, NY 13244
[23]University of Illinois, Urbana-Champaign, IL 61801
[24]University of Massachusetts, Amherst, MA 01003
[25]Norfolk State University, Norfolk, VA 23504
[26]Universität Basel, CH-4056 Basel, Switzerland
[27]Old Dominion University, Norfolk, VA 23529
[28]Temple University, Philadelphia, PA 19122
[29]Budker Institute for Nuclear Physics, Novosibirsk 630090, Russia
[30]Tel Aviv University, Tel Aviv, 69978 Israel
[31]Duke University and TUNL, Durham, NC 27708
[32]Kyungpook National University, Taegu City, South Korea
[33]Institute for Nuclear Physics, Tomsk 634050, Russia
[34]Instituto de Estructura de la Materia, Madrid, Spain

(Dated: May 28, 2010)

The electric form factor of the neutron was determined from studies of the reaction $^3\overrightarrow{\mathrm{He}}(\vec{\mathrm{e}},\mathrm{e'n})\mathrm{pp}$ in quasi-elastic kinematics in Hall A at Jefferson Lab. Longitudinally polarized electrons were scattered off a polarized target in which the nuclear polarization was oriented perpendicular to the momentum transfer. The scattered electrons were detected in a magnetic spectrometer in coincidence with neutrons that were registered in a large-solid-angle detector. More than doubling the Q^2-range over which it is known, we find $G_E^n = 0.0219 \pm 0.0016(stat) \pm 0.0022(syst)$, $0.0212 \pm 0.0025 \pm 0.0017$, and $0.0143 \pm 0.0019 \pm 0.0013$ for $Q^2 = 1.72$, 2.48, and 3.41 GeV^2, respectively.

PACS numbers: 14.20.Dh, 13.40.Gp, 24.70.+s, 25.30.Bf

Understanding the nucleon in terms of QCD degrees of freedom requires precision measurements of nucleon structure, including the form factors (FFs) that govern the elastic scattering of electrons. Important advances in such efforts came from the determination, at Jefferson Laboratory (JLab), of the ratio of the electric and magnetic elastic FFs of the proton, G_E^p/G_M^p, over a range of the four-momentum transfer squared (Q^2) of 1 to 6 GeV^2 [1]. The ratio G_E^p/G_M^p was observed to decrease almost linearly with increasing Q^2, when expectations, based on both earlier cross-section measurements and theoretical models of the nucleon, had been that such a ratio is constant. This observation has clarified the necessity for a reconsideration of nucleon structure with an increased emphasis on the significance of quark orbital angular momentum (OAM), see e.g. the review [2]. Evidence of quark OAM has subsequently been observed in several other independent contexts [3]. Given the important implications of Ref. [1], it is critical to determine the neutron form-factor ratio, $g_n \equiv G_E^n/G_M^n$, in a Q^2-region where the unexpected results for the proton were observed, and thus test the theoretical explanations that have emerged for the proton data.

The powerful method of determining FFs using double-polarization asymmetries [4], which led to the striking results of [1], has also been used to study g_n up to Q^2=1.5 GeV^2. These experiments have employed polarized electrons and either a neutron polarimeter [5, 6], a polarized deuteron target [7, 8], or a polarized ^{3}He target [9–12]. At low momentum transfer, the nuclear effects in double-polarization asymmetries have been taken into account using precise non-relativistic three-body calculations based on the Faddeev-like integral equations [13], whereas, at large Q^2, the eikonal approximation [14] provides sufficient precision. For Q^2-values of several GeV^2, however, even polarization-based studies of g_n become very challenging due to the small cross sections involved, thus necessitating significant technical development.

We report a measurement of g_n up to Q^2=3.4 GeV^2 performed at JLab in experimental Hall A. The experiment was made possible by the use of a high-luminosity optically-polarized ^{3}He target, a magnetic spectrometer of 76 msr solid angle to detect the scattered electrons, and a large neutron detector with matched acceptance. The typical ^{3}He-electron luminosity was 5×10^{35} neutron/cm$^2 \times$ electron/s. The central kinematics, as well as the average values of various experimental parameters, are listed in Table I.

The experiment, E02-013, used a longitudinally polarized electron beam with a current of up to 8 μA. The helicity of the beam was pseudo-randomly flipped at a rate of 30 Hz. The helicity-correlated charge asymmetry was monitored and kept below 0.01%. The beam polarization, monitored continuously by a Compton polarimeter, and measured several times by a Møller polarimeter [15], was determined with a relative accuracy of 3%.

TABLE I: Kinematics and other relevant parameters of the experiment: the four-momentum transfer, Q^2; beam energy, E_{beam}; central angle of the electron spectrometer, θ_e; central angle of the neutron detector, θ_n; distance from the target to the neutron detector, D; longitudinal beam polarization, P_e; target polarization, P_{He}.

$\langle Q^2 \rangle$	[GeV^2]	1.72	2.48	3.41
E_{beam}	[GeV]	2.079	2.640	3.291
θ_e	[deg]	51.6	51.6	51.6
θ_n	[deg]	33.8	29.2	24.9
D	[m]	8.3	11	11
$\langle P_e \rangle$	[%]	85.2	85.0	82.9
$\langle P_{He} \rangle$	[%]	48.5	45.2	47.7

The polarized ^{3}He target, while similar in many respects to the target described in Ref. [15], included several important improvements. The ^{3}He was polarized by spin-exchange with an optically pumped alkali vapor, but unlike earlier targets at JLab, the alkali vapor was a mixture of Rb and K [16], rather than Rb alone. This greatly increased the efficiency of spin transfer to the ^{3}He nuclei, resulting in a significantly higher polarization (∼50%) and reduced sensitivity to depolarization by the beam. The ^{3}He gas (at a pressure of ∼10 atm), a 1% admixture of N_2 (to aid in the optical pumping process), and the alkali vapor were contained in a sealed glass cell with two chambers. The portion of the cell in the electron beam was a cylinder 40 cm in length and 2 cm in diameter. The polarization of the target was measured every six hours using NMR, with relative accuracy of 4%, and was calibrated using a technique based on electron paramagnetic resonance [17]. A magnetic field of 25 G was created in the target area by means of a 100 cm gap dipole magnet. The horizontal direction of the field in the target area, 118° with respect to the electron beam, was nearly orthogonal to the momentum-transfer vector and was measured to 1 mrad accuracy. Additional targets used in the experiment included a set of nine carbon and BeO foils, spaced by 6.7 cm, and a reference cell, which could be filled with H_2 or N_2. The target cell alignment along the beam and the potential scraping of the beam by the cell walls was regularly investigated by varying the size of the electron beam spot.

The scattered electrons were detected in the BigBite spectrometer, originally used at NIKHEF-K [18]. It consisted of a dipole magnet and a detector stack subtending a solid angle of 76 msr for a 40 cm long target. For this experiment, the detector package was completely rebuilt to accommodate an increase in luminosity of 10^5. The spectrometer was equipped with 15 planes of high-resolution, high-segmentation multi-wire drift chambers, a two-layer lead-glass calorimeter for triggering and pion rejection, and a scintillator hodoscope for event timing information. BigBite provided a relative momentum resolution of $\sim$1% for electrons with a momentum of 1.5 GeV/c, a time resolution of 0.25 ns, and an angular resolution of 0.3 (0.7) mrad in the vertical (horizontal) direction. The Q^2-acceptance was $\sim$10% of the Q^2-value despite the large angular acceptance of BigBite, thanks to its large 5:1 vertical/horizontal aspect ratio.

The recoiling nucleons were detected in coincidence using a large hadron detector, BigHAND, that included (moving downstream from the target) two planes of segmented veto counters, a one-inch lead shield, and seven layers of neutron counters. Each neutron-counter layer covered a $1.7 \times 4\,\mathrm{m}^2$ area and was comprised of 25(40) plastic scintillator counters that were 5(10) cm thick. All counters were oriented horizontally except for a set of narrow vertical bars that were used to calibrate the horizontal coordinate measurement. A time-of-flight (ToF) resolution of 0.40 ns was achieved, and the coordinate resolution was 5 cm. The efficiency of each veto plane was found to be 97%. The detector was shielded on the target side with 5 cm of lead and 1 cm of iron and on all other sides with 5 cm of iron.

The trigger was formed using a 100 ns wide coincidence between the signals from BigHAND and BigBite, and required the total energy in the BigHAND scintillator counters to be above 25 MeV and the total energy deposited in the BigBite calorimeter to be above 500 MeV. Monte Carlo simulations of the detector response, developed within the framework of Geant4, produced results which were found to be in good agreement with the detector characteristics obtained from the experimental data.

The BigBite spectrometer optics were used to reconstruct the momentum, direction, and the reaction vertex of the electrons. BigHAND was used to determine the direction, ToF, and charge of the recoiling particle. Using BigBite, it was also possible to accurately determine the time at which the scattering event took place, which in turn provided the start time for computing the ToF, and hence the momentum, p_n, of the recoil nucleon. The three-momentum transfer, $\vec{q}$, was used to calculate, for the recoil nucleon, the missing perpendicular momentum, $p_{\perp} = |(\vec{q} - \vec{p}_n) \times \vec{q}|/|\vec{q}|$ and the missing parallel momentum, $p_{\parallel} = (\vec{q} - \vec{p}_n) \cdot \vec{q}/|\vec{q}|$. The invariant mass of the system comprised of the virtual photon and the target nucleon (assumed to be free and at rest), W, was calculated as $W = \sqrt{m^2 + 2\,m\,(E_i - E_f) - Q^2}$, where m is the neutron mass, E_i the beam energy, and E_f the energy of the detected electron. The identification of quasi-elastic events was largely accomplished using cuts on $p_{\perp}$ and W. Additional cuts included the nucleon $p_{\parallel}$ and the total mass of the undetected hadrons.

The measured asymmetry was calculated as:

$$A^{p(a)}_{meas} = \frac{1}{P_e\,P_{_{He}}}\left[\frac{N^{p(a)}_{+} - N^{p(a)}_{-}}{N^{p(a)}_{+} + N^{p(a)}_{-}}\right],$$

where $N^{p(a)}_{h}$ was the number of events with the target polarization parallel (anti-parallel) to the vector of the holding magnetic field, and beam helicity h. An appropriate average of A^{p}_{meas} and A^{a}_{meas}, A_{meas}, was used in the g_n analysis. In the case of the elastic scattering of 100% longitudinally polarized electrons off a free 100% polarized neutron, in the one-photon approximation, g_n is related to the double spin asymmetry, A_{en}, through [19]

$$A_{en} = \frac{-2\sqrt{\tau(\tau+1)}\tan(\theta_e/2)\,\cos\phi^*\sin\theta^*\,g_n}{g_n^2 + \tau\left[1 + 2(1+\tau)\tan^2(\theta_e/2)\right]} + \frac{-2\tau\sqrt{1+\tau+(\tau+1)^2\tan^2(\theta_e/2)}\tan(\theta_e/2)\,\cos\theta^*}{g_n^2 + \tau\left[1 + 2(1+\tau)\tan^2(\theta_e/2)\right]},$$

where $\tau = Q^2/4m^2$, θ^* is the angle between the direction of the ^{3}He polarization and $\vec{q}$, and ϕ^* is the angle between the electron scattering plane and the $(\vec{p}_n, \vec{q})$ plane.

To obtain g_n from A_{meas} a number of corrections were applied, the most important of which are presented in Table II. A target dilution factor, D_t, was applied to account for scattering from the N_2 admixture in the target gas. The contribution from accidental coincidences was calculated by using the interval of the ToF spectrum which was free from real coincidence events. The accidental events introduced a background dilution, D_{bkgr}, which had an asymmetry A_{bkgr}. After correction for this background, the resulting physical asymmetry, A_{phys},

TABLE II: Data analysis parameters and the resulting asymmetry values used to calculate $\mu_n G^n_E/G^n_M$.

$\langle Q^2\rangle$ [GeV^2]	1.72	2.48	3.41
W [GeV]	0.7-1.15	0.65-1.15	0.6-1.15
$p_{\perp}$ [GeV]	< 0.15	< 0.15	< 0.15
A_{meas}	-0.132	-0.130	-0.095
D_t	0.948	0.949	0.924
D_{bkgr}	0.970	0.981	0.975
A_{bkgr}	0.000	-0.001	-0.001
A_{phys}	-0.143	-0.140	-0.106
A_{QE}	-0.144	-0.136	-0.105
$D_{p/n}$	0.796	0.757	0.797
A_{ep}	-0.010	-0.008	-0.006
$A_{en}\|_{exp}$	-0.179	-0.178	-0.131

was calculated. A_{phys} was corrected for inelastic single-pion electroproduction events that remained in the event sample after the W cut because of the non-zero initial momentum of the neutrons. Such a correction, calculated with the MAID parameterization [20] using PWIA, resulted in the value of the asymmetry for the quasi-elastic events, A_{QE}.

The final steps in extracting g_n involve calculations of the asymmetries in the quasi-elastic processes $^3\overrightarrow{\mathrm{He}}(\vec{e},e'n)pp$ and $^3\overrightarrow{\mathrm{He}}(\vec{e},e'p)np$. These calculations were performed using the generalized eikonal approximation (GEA) [21], and included the spin-dependent final-state interactions and meson-exchange currents, and used the ^{3}He wave function that results from the CD-Bonn potential [22]. The yield of the quasi-elastic events and the asymmetries were calculated vs. W and an assumed value of g_n with the values for other nucleon FFs from [23]. The estimated accuracy of these calculations is 2% [24]. The acceptance of the experimental setup, orientation of the target polarization, and the cuts applied to $p_\perp$ and $p_\parallel$ were all taken into account. We note that the effective neutron polarization in our final event sample, as calculated in the PWIA approximation, was greater than ∼96% of P_{He} (in agreement with [25]) due to our selection of events with small $p_\perp$. The asymmetries for $^3\overrightarrow{\mathrm{He}}(\vec{e},e'n)pp$ calculated within GEA were found to be within 3% of the PWIA values, indicating that nuclear re-scattering effects were quite small.

The asymmetry $A_{en}|_{exp}$ was obtained from the A_{QE} by correcting for a dilution due to protons in the sample of quasi-elastic events that remained after applying the proton-rejection cuts. The dilution factor, $D_{p/n}$, was found by comparing data collected from three targets (H_2, ^{3}He, and N_2), together with a Monte Carlo simulation of the experiment. The asymmetry A_{ep} used for this correction was an average of the GEA result and the experimental value. The difference between them was included as a systematic uncertainty. The experimental value of g_n and its statistical uncertainty were calculated by comparing $A_{en}|_{exp}$ with the asymmetries from GEA [24]. The systematic uncertainty was obtained by combining in quadrature the contributions of individual effects (the largest of which are described above).

Our results for $\mu_n G_E^n/G_M^n$ are shown in Fig. 1 along with recent data sets that extend beyond Q^2=0.5 GeV^2 [5–8, 12]. It is important to compare our results with calculations that have described well the proton FF data. Three such calculations are shown in Fig. 1. In all of them, quark OAM plays an important role. One is a logarithmic scaling prediction $F_2/F_1 \propto \ln^2(Q^2/\Lambda^2)/Q^2$ [26], based on pQCD, which is shown for two values of the soft-scale parameter Λ. It is in clear disagreement with the combined neutron data, despite providing a good description of the proton data (and the neutron data of [6]). The authors of [26] noted, however, that the agreement with the proton data may

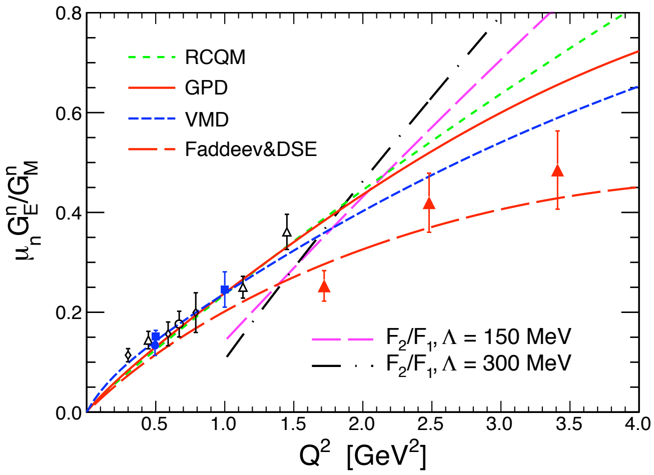

FIG. 1: The ratio of $\mu_n G_E^n/G_M^n$ vs. the momentum transfer with results of this experiment (solid triangles) and selected published data: diamonds [5], open triangles [6], circles [7], squares [8], open circles [12], and calculations: (F_2/F_1) [26], (RCQM) [27], (Faddeev&DSE) [28], (GPD) [29], and (VMD) [30]. The curves labeled F_2/F_1 present a prediction [26] normalized to 0.3 at Q^2=1.5 GeV^2. The error bars for our data show the statistical and the systematic uncertainties added in quadrature.

well have been due to delicate cancellations, given the relatively low values of Q^2 involved. Another calculation is the Light Front Cloudy Bag Model [27], an example of a relativistic constituent quark model (RCQM) calculation that, in this case, includes a pion cloud. This RCQM anticipated the observed decreasing Q^2 dependence of G_E^p/G_M^p. Finally, we show a calculation based on QCD's Dyson-Schwinger equations [28], in which the mass of the quark propagators is dynamically generated. Both of these last two calculations appear to have reasonable qualitative agreement with the world data for g_n, althrough that of [28] is closest to our results. Also shown in Fig. 1 are the predictions based on GPDs [29] and Vector Meson Dominance [30] that were fit to the data that were available prior to this work.

Flavor-separated Dirac and Pauli FFs of the nucleon, $F_{1,2}^d$ and $F_{1,2}^u$, can be obtained from the electric and magnetic FFs of the proton and the neutron, assuming isospin symmetry and neglecting the contribution of the strange quark FFs [31]. Experimental data (as shown in Fig. 1) for g_n and the Kelly fit for G_E^p, G_M^p and G_M^n [23] were used to compute the ratios F_1^d/F_1^u and $\kappa_d^{-1}F_2^d/\kappa_u^{-1}F_2^u$ (in the proton), where κ_d, κ_u are the anomalous magnetic moments of the u and d quarks, respectively. As shown in Fig. 2, the ratio F_1^d/F_1^u exhibits a trend downward with an increase of Q^2. This means that the corresponding infinite-momentum-frame charge density [32] of the d quark as a function of impact parameter is significantly broader than that of the u quarks. Such an experimental result is related to the established decrease of the quark PDF ratio, d/u, with increasing x_{Bj}. The calculations discussed earlier, as well as the recent lattice

TABLE III: Experimental results for G_E^n/G_M^n and G_E^n (using linearly interpolated values of G_M^n from [34]).

$\langle Q^2 \rangle$ [GeV^2]	range, ΔQ^2 (rms), [GeV^2]	G_E^n/G_M^n $\pm$ stat. $\pm$ syst.	$G_E^n$$\pm$ stat. $\pm$ syst.
1.72	0.14	$-0.132 \pm 0.010 \pm 0.013$	$0.0219 \pm 0.0016 \pm 0.0022$
2.48	0.18	$-0.220 \pm 0.026 \pm 0.017$	$0.0212 \pm 0.0025 \pm 0.0017$
3.41	0.22	$-0.254 \pm 0.034 \pm 0.022$	$0.0143 \pm 0.0019 \pm 0.0013$

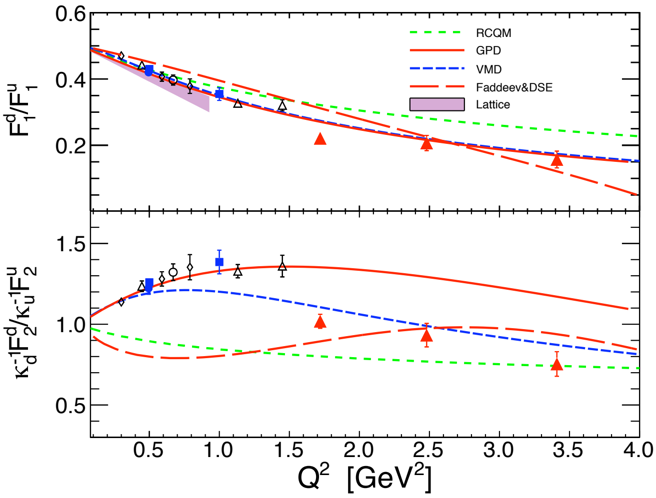

FIG. 2: Nucleon flavor FF ratios F_1^d/F_1^u and $\kappa_d^{-1}F_2^d/\kappa_u^{-1}F_2^u$ vs Q^2, where κ_d, κ_u are the anomalous magnetic moments of the u and d quarks, respectively. The band indicates the lattice QCD result [33]. Data and curves as in Fig. 1.

QCD results [33], are in good agreement with experimental data for F_1^d/F_1^u. Also shown in Fig. 2 is the ratio $\kappa_d^{-1}F_2^d/\kappa_u^{-1}F_2^u$, which becomes significantly smaller than the GPD fit prediction [29] above Q^2=1.5 GeV^2. Such a discrepancy evidently necessitates a re-fit of the GPD model parameters, which could significantly change the spin-flip GPDs $E_{u,d}$.

We conclude by summarizing in Table III our experimental results. This experiment more than doubles the Q^2-range over which G_E^n is known, greatly sharpens the mapping of the nucleon's constituents and provides a new benchmark for comparison with theory.

We thank the Jefferson Lab Hall A technical staff for their outstanding support. This work was supported in part by the National Science Foundation, the U.S. Department of Energy and the UK Engineering and Physical Science Research Council. Jefferson Science Associates, LLC, operates Jefferson Lab for the U.S. DOE under U.S. DOE contract DE-AC05-060R23177.

* Corresponding author: bogdanw@jlab.org
† Deceased

[1] M.K. Jones *et al.*, Phys. Rev. Lett. **84**, 1398 (2000); O. Gayou *et al.*, Phys. Rev. Lett. **88**, 092301 (2002).
[2] S. Boffi and B. Pasquini, Riv. Nuovo Cim., **30**, 387 (2007).
[3] X. Zheng *et al.*, Phys. Rev. Lett. **92**, 012004 (2004); A. Airapetian *et al.*, Phys. Rev. Lett. **103**, 152002 (2009).
[4] A.I. Akhieser, L.N. Rozenzweig and I.M. Shmushkevich, Sov. Phys. JETP **6**, 588 (1958); R.G. Arnold, C.E. Carlson, and F. Gross, Phys. Rev. C **23**, 363 (1981).
[5] D.I. Glazier *et al.*, Eur. Phys. J **A** **24**, 101 (2005).
[6] B. Plaster *et al.*, Phys. Rev. C **73**, 025205 (2006).
[7] H. Zhu *et al.*, Phys. Rev. Lett. **87**, 081801 (2001);
[8] G. Warren *et al.*, Phys. Rev. Lett. **92**, 042301 (2004).
[9] C.E. Jones-Woodward *et al.*, Phys. Rev. C **44**, R571 (1991).
[10] J. Becker *et al.*, Eur. Phys. J. A **6**, 329 (1999).
[11] J. Golak *et al.*, Phys. Rev. C **63**, 034006 (2001).
[12] D. Rohe *et al.*, Phys. Rev. Lett. **83**, 4257 (1999); J. Bermuth *et al.*, Phys. Lett. B **564**, 199 (2003).
[13] W. Glöckle *et al.*, Phys. Rep. **274**, 107 (1996); H. Witala *et al.*, Phys. Rev. C **63**, 024002 (2001).
[14] R.J. Glauber, Phys. Rev. **100**, 242 (1955).
[15] J. Alcorn *et al.*, Nucl. Instrum. Methods Phys. Res., Sect. A **522**, 294 (2004).
[16] W. Happer, G.D. Cates, M.V. Romalis, and C.J. Erickson, U.S. Patent No. 6,318,092 2001; E. Babcock *et al.*, Phys. Rev. Lett. **91**, 123003 (2003).
[17] M.V. Romalis and G. Cates, Phys. Rev. A **58**, 3004 (1998).
[18] D.J.J. de Lange *et al.*, Nucl. Instrum. Methods Phys. Res., Sect. A **406**, 182 (1998).
[19] T.W. Donnelly and A.S. Raskin, Ann. Phys. (N.Y.) **169** 247 (1986).
[20] D. Drechsel, S.S. Kamalov, and L. Tiator, Nucl. Phys. **A**645, 145 (1999) and Eur. Phys. J. **A** 34, 69 (2007).
[21] M. Sargsian *et al.*, Phys. Rev. C **71**, 044614 (2005).
[22] R. Machleidt, Phys. Rev. C **63**, 024001 (2001).
[23] J.J. Kelly, Phys. Rev. C **70**, 068202 (2004).
[24] M. Sargsian, private communication (2010).
[25] J. Carlson and R. Schiavilla, Reviews of Modern Physics, **70**(3), 743 (1998).
[26] A.V. Belitsky, X. D. Ji, and F. Yuan, Phys. Rev. Lett. **91**, 092003 (2003).
[27] G.A. Miller, Phys. Rev. C **66**, 032201(R) (2002); H.H. Matevosyan, A.W. Thomas, G.A. Miller, Phys. Rev. C **71**, 065204 (2005); private communication (2009).
[28] C.D. Roberts *et al.*, Eur. Phys. J. **ST** **140**, 53 (2007); I.C. Cloët *et al.*, Few-Body Systems **46**, 1(2009).
[29] M. Diehl *et al.*, Eur. Phys. J. C **39**, 1 (2005); M. Guidal *et al.*, Phys. Rev. D **72**, 054013 (2005).
[30] E.L. Lomon, Phys. Rev. C **66**, 045501 (2002); arXiv:nucl-th/0609020.
[31] G.A. Miller, B.M.K. Nefkens, and I. Slaus, Phys. Rep. **194**, 1 (1990).
[32] G.A. Miller, Phys. Rev. Lett. **99**, 112001 (2007).
[33] J.D. Bratt *et al.*, arXiv:1001.3620.
[34] J. Lachniet *et al.*, Phys. Rev. Lett. **102**, 192001 (2009).